LA-UR-14-24929
Approved for public release; distribution is unlimited.

Title: Ceria and Doped Ceria Nanoparticle Additives For Polymer Fuel Cell Lifetime Improvement

Author(s): Stewart, S. Michael
Borup, Rodney L.
Wilson, Mahlon S.
Datye, Abhaya
Garzon, Fernando H.

Intended for: Transactions of The Electrochemical Society
226th Meeting of The Electrochemical Society, 2014-10-05/2014-10-10 (Cancun, Mexico)

Issued: 2014-07-02 (Draft)

Ceria and Doped Ceria Nanoparticle Additives For Polymer Fuel Cell Lifetime Improvement

S. Michael Stewart,[a] Rodney Borup,[b] Mahlon Wilson,[b]
Abhaya Datye,[c] Fernando Garzon[b]
[a] Dept. Of Materials Science & Engineering, Stanford University, Stanford, CA
[b] Los Alamos National Laboratory, Los Alamos, NM
[c] Department of Chemical & Biological Engineering, University of New Mexico, Albuquerque, NM

Polymer electrolyte fuel cell membranes are degraded by oxygen free radical attack. The addition of cerium oxide and doped cerium oxide nanoparticles improves membrane stability as measured by open circuit voltage and low humidity accelerated stress testing. In this work we varied the crystallite size of ceria nanoparticles and investigated their role in enhancing durability of the PEM fuel cell. We found that the ratio of the free radical production to hydrogen peroxide decomposition rates provides a novel approach to characterize the efficiency of free radical scavenging catalysts. Nanoparticle crystallite size and doping plays a significant role in determining the surface area normalized efficiency of ceria based free radical scavengers.

Introduction

Polymer electrolyte fuel cell (PEFC) membrane durability is limited by free radical attack generated from oxygen reduction processes (1,2). The creation of peroxide via two electron oxygen reduction and subsequent decomposition into hydroxyl and/or hydroperoxyl free radicals may be the major source of nonmetallic fuel cell component chemical degradation. The addition of Ce^{+3} by ion exchange has greatly improved the durability of PEFCs (3). The cerium cations decompose the free radical species at high rates, thus limiting membrane damage and carbon support oxidation. An alternative approach is the addition of cerium oxide nanoparticles as free radical scavengers. The surfaces of CeO_2 nanoparticles contain appreciable concentrations of Ce^{+3} and Ce^{+4} that may act as catalytic sites for free radical decomposition. However little is known about the effects of particle size and doping on the free radical scavenging rates, and the selectivity towards peroxide decomposition versus secondary free radical generation has not been previously studied.

Experimental

Nano Ceria Synthesis and Characterization

Ceria and *M*-doped ceria (*M*=Pr, Zr) nanoparticles of ~ 5-40 nm crystallite sizes were synthesized using acetate solution precursors. Cerium(III) acetate (Strem Chemicals) and

Pr, or Zr acetates were dissolved in deionized water acidified to obtain a solution of 0.1 M metal ions (Ce + *M*),. To the mixture concentrated nitric acid (Fisher) was added until both the cerium and *M* acetates were dissolved (pH = 1). Once both metal acetates were fully dissolved, a 50 % ammonium hydroxide solution (Alfa-Aesar) was added to the solution while manually agitated until the solution turned white and opaque (pH ~ 10). The solution was centrifuged, and then washed with DI water three times to remove acetate, ammonia, and nitric acid contaminants. Samples were then dried in an oven at 140 °C for one hour to remove moisture. The dried samples were subsequently transferred to a ceramic boat and heated under air at between 200 -800 °C for 1 hour to achieve a range of particles sizes from 5 to 40 nm.

Phase purity, crystal structure, lattice parameters and crystallite size were determined by powder X-Ray Diffraction (XRD) with a Siemens D5000 using a Cu Kα source operating at 40 kV and 35 A. Powder samples were dispersed across a zero background quartz sample holder using acetone. 2 mm anti-scatter slits were used to define the illuminated sample area, with a 0.6 mm detector slit. Samples were measured from 10° to 120° 2θ at 0.02° step size. Data analysis was performed using Whole Profile fitting Refinement methods with Jade 9 (MDI) software.

Specific (normalized to BET surface area) hydrogen peroxide decomposition rates were measured by volumetric determination of catalytic oxygen production. Approximately fifty milligrams of sample, with the mass used varied to have approximately the same amount of accessible surface area across the experiments, was added to 1 mL of deionized water and stirred with a magnetic stir bar for one minute to disperse the nanoparticles. 30 % hydrogen peroxide (Sigma Aldrich) was added to the nanoparticle-water mixture and evolved oxygen was measured by water displacement from an inverted burette. The amount of oxygen evolved was measured every five minutes, and the resulting oxygen volume versus time was fit to a first order exponential decay to calculate the rate at time zero. The observed rate constant was normalized to the surface area of the catalyst used.

To determine the peroxide decomposition to free radical production selectivity, a process similar to the method used by Prabhakaran, et al., was employed (4). Summarized briefly, 23.5 mg of 6-carboxyfluoroscein (6CF, Sigma-Aldrich) was added to 250 mL of 1 % hydrogen peroxide. 30 mL of the 6CF-peroxide solution was introduced to an open beaker, to which was added less than fifty milligrams of sample; as with the peroxide, the amount of sample added was scaled to maintain the same accessible surface area between samples. A multidiode UV-vis spectrometer (Hewlett Packard) was used to quantify the amount of 6CF remaining in solution by measurement of the decay of the 492 nm peak. Measurements were taken every five minutes for an hour, and the loss of 6CF was fit to a first order exponential decay. This rate was normalized to the nitrogen BET accessible surface area of the catalyst used. The inverse selectivity; the normalized rate of 6CF decomposition divided by the normalized rate of oxygen evolution, is reported because the selectivity would go to infinity for catalysts which show zero free radical production rate.

Fluorine ion emission rates were determined by fluorine Ion Specific Electrode (Orion). Anode and cathode water samples were collected by condensation, and mixed with ORION® Total Ionic Strength Adjustment Buffer (TISAB II) solution and fluorine ion concentration was measured using the potentiometric method.

Ink Synthesis and Membrane Electrode Assembly (MEA) Construction

Inks were made by mixing 2 % Nafion© solution with a TKK platinum supported on carbon catalyst (47.9 wt% Pt) and stirring for an hour in a scintillation vial. Subsequently, glycerol was added at 50 % of the total weight of the Nafion© solution, and the mixtures were stirred for another hour. Next, tetra-butylammonium was added at 5 % of the total weight of the Nafion© solution, and the mixture was stirred for another hour. If pure or mixed ceria (2% of the weight of platinum) were also added to the cathode inks, they were incorporated after the tetra-butylammonium was stirred into the Nafion© solution and the mixtures were stirred overnight. Decals were made by painting catalyst inks onto 50 cm^2 polymer substrates. The loading of platinum as well as the platinum to cerium ratio was verified using X-ray Fluorescence Spectroscopy (Spectrace QuantX); all cathode decal loadings were 0.23 mg Pt/cm^2 and the anode decal loadings were 0.18 mg Pt/cm^2.

50 cm^2 active-area MEAs were assembled on site using 10x10 cm Dupont Nafion© XL proton exchange membranes. To create un-stabilized MEAs, the XL membranes were first boiled in 1 M NaOH for two hours, then in deionized water for two hours, and left to cool in deionized water overnight. The washed membranes were partially dried at 80°C for 10 minutes, then hot pressed between the decals at 120 psi/cm^2 at 212 °C for 5 minutes, then allowed to cool to room temperature in air. The pressed MEAs were boiled in 1 M sulfuric acid for two hours, then in deionized water for two hours, and left to cool in deionized water overnight. The removal of the silica and cerium ions was confirmed by XRF and EDS measurements. Fuel cells were assembled using SGL 25BC gas diffusion layers (SGL Group) with graphite serpentine flow-field plates.

Accelerated Stress Testing (AST) of Fuel Cells

Open circuit voltage testing at low relative humidity (RH) is well known to accelerate membrane degradation. Cells were conditioned by operating at 80 °C and 100 % RH overnight. Beginning of life testing was carried out after conditioning at both 30 °C and 100 % RH, and 80 °C and 30 % RH. For beginning of life testing, the high frequency resistance, limiting current, power-density, and impedance spectroscopy were performed with hydrogen, 700 sccm flow/1.7 bar backpressure and air, 1669 sccm flow/1.2 bar. Hydrogen crossover, and cyclic voltammetry were measured at a 500 sccm gas flow/0.25 bar with hydrogen reference gas and nitrogen gas at the working electrode. The cells were allowed to operate under open circuit at 80 °C, 30 % RH, except when tested every 24 to 72 hours to assess cell degradation. Jacketed condensers were used to remove water vapor from the exhaust gases for measurements of the anode and cathode fluorine emission rates. The AST's were stopped when open circuit potential dropped beneath 0.7 V, at which point impedance spectroscopy and limiting current measurements were impossible, or the crossover current appeared ohmic, which was indicative of a gas crossover leak in the cell.

Unmodified Dupont Nafion XL membranes containing both cerium cations and silica fibers as-received, were also subjected to stress testing to determine baseline behavior. Unlike the destabilized membranes, the control XL membranes were not pretreated by boiling in sodium hydroxide or sulfuric acid. The as-received membranes were used to fabricate MEAs using ink decal transfer, and then conditioned and tested in the same manner as the other cells.

A FEI Quanta 400F Scanning Electron Microscope (SEM) equipped with a Thermo Noran Energy Dispersive Spectrometer (EDS) was used to acquire SEM images of membranes after conditioning and stress testing. A typical MEA was submerged in liquid nitrogen and cut using a fresh razor blade from the anode side of the MEA to minimize the amount of catalyst pushed into the PEM by the edge of the blade. 5 keV electrons were used, and both backscattered (BSE) and secondary electrons (SE) images were recorded.

Results

Figures 1 and 2 show the inverse selectivity versus H_2O_2 oxidation reactivity for praseodymium and zirconium doped cerium oxides respectively. On each plot, the performance of cerium oxide is plotted in red for comparison. An ideal catalyst would be one that maximizes reactivity while minimizing inverse selectivity; the particle size that gives the fastest peroxide decomposition rate while producing the least free radicals.

Un-doped cerium oxide exhibits interesting trends in specific activity and inverse selectivity. The red markers representing the pure ceria samples, clearly show a trend of increasing area specific activity with decreasing particle size, however the free radical production rate increases for the smaller ~ 8 to 5nm particle size range. The largest particle sizes produce no measurable free radicals, however it is desirable for fuel cell performance to minimize the volume of MEA components that do not contribute to multiphase transport.

As compared to pure cerium oxide, when praseodymium is incorporated into the nanoparticle at 5 at%, the optimal reactivity is seen for circa 7 nm without any loss in selectivity, with smaller and larger crystallite sizes giving worse activity. Similarly for 15 at% Pr incorporation, the optimal crystallite size is closer to 6 nm with a loss of activity and selectivity seen above and below this crystallite size. For the 15 at% Pr particles, the activity and selectivity of the particles approaches that of pure praseodymium for the 22.3 nm particles, whereas the 5 at% Pr particles, while beginning to become less selective and active for larger crystallite sizes, do not reproduce the behavior of pure praseodymium at 17.1 nm. However, the 5 at% particles give better performance over pure cerium oxide and 15 at% nanoparticles. For zirconium doping, unlike praseodymium, there is no loss in activity and selectivity with decreasing crystallite size as seen in Figure 2. In fact, decreasing particle size and increasing zirconia content improve both activity and selectivity in these nanoparticles, and suggests

that any cerium-zirconium nanoparticles beneath 7 nm would be useful for selectively decomposing hydrogen peroxide.

When compared to a destabilized membrane cell, large cerium oxide nanoparticle have stabilizing effects, which results in a lower loss in performance over time. Both medium and small cerium oxide nanoparticles also show some initial stabilization. However, ultimately they have a detrimental effect on the lifetime of the fuel cells during accelerated stress testing, causing increases in hydrogen cross over and fluorine emission, and an exponential loss in open circuit voltage. As predicted from selectivity and activity performance, ~ 7.0 nm pure cerium oxide nanoparticles incorporated in the cathode catalyst layer impart the same initial stabilization for fuel cells as cerium cations dispersed in the membrane; Figures 3 and 4 illustrate this effect. However, this improvement is short lived. The loss in performance is attributed to the loss of cerium oxide due to dissolution, which increases for decreasing particle size (5). After 350 hrs the cerium oxide particle sizes become smaller, perhaps changing the energetics of the cerium oxide oxidation states, so that the selectivity of the cerium oxide for free radical decomposition becomes too low and the peroxide decomposition on cerium oxide generates an increasing amount of free radicals. A parallel study by the authors using spatially resolved XRF, observed cerium migration in both Ce^{+3} ion exchanged membrane fuel cells and ceria nanoparticle stabilized fuel cells after accelerated stress testing in very short time periods (6).

Conclusions

While future work remains on the stabilization effects of zirconium doped cerium oxide nanoparticles in fuel cells, research focusing on the changes in selectivity and activity of doped nanoparticles for hydrogen peroxide decomposition provided insight into their predicted behavior. Of the two dopants, partial substitution of zirconium for cerium demonstrated ideal behavior; increasing selectivity and activity with decreasing particles size, with no observed lower limit on particle size.

In conclusion, the nanoparticle additives were shown to decompose peroxide and in some cases, improve ionomer durability. The catalytic activity and reaction pathway of cerium oxide towards hydrogen peroxide decomposition was strongly influenced by the crystallite size and the doping of cerium oxide nanoparticles. For both cerium oxide and doped cerium oxide, the size and doping of ceria nanoparticles are also shown to play an important role in their ability to improve membrane durability. However, the materials used in this study are not sufficiently optimized to compete yet with commercial ion exchange stabilized membranes. Future work must focus on understanding the mechanism of free radical elimination on ceria surfaces, as well as understanding why dopants and particle size strongly impact the selectivity of the ceria nanoparticles.

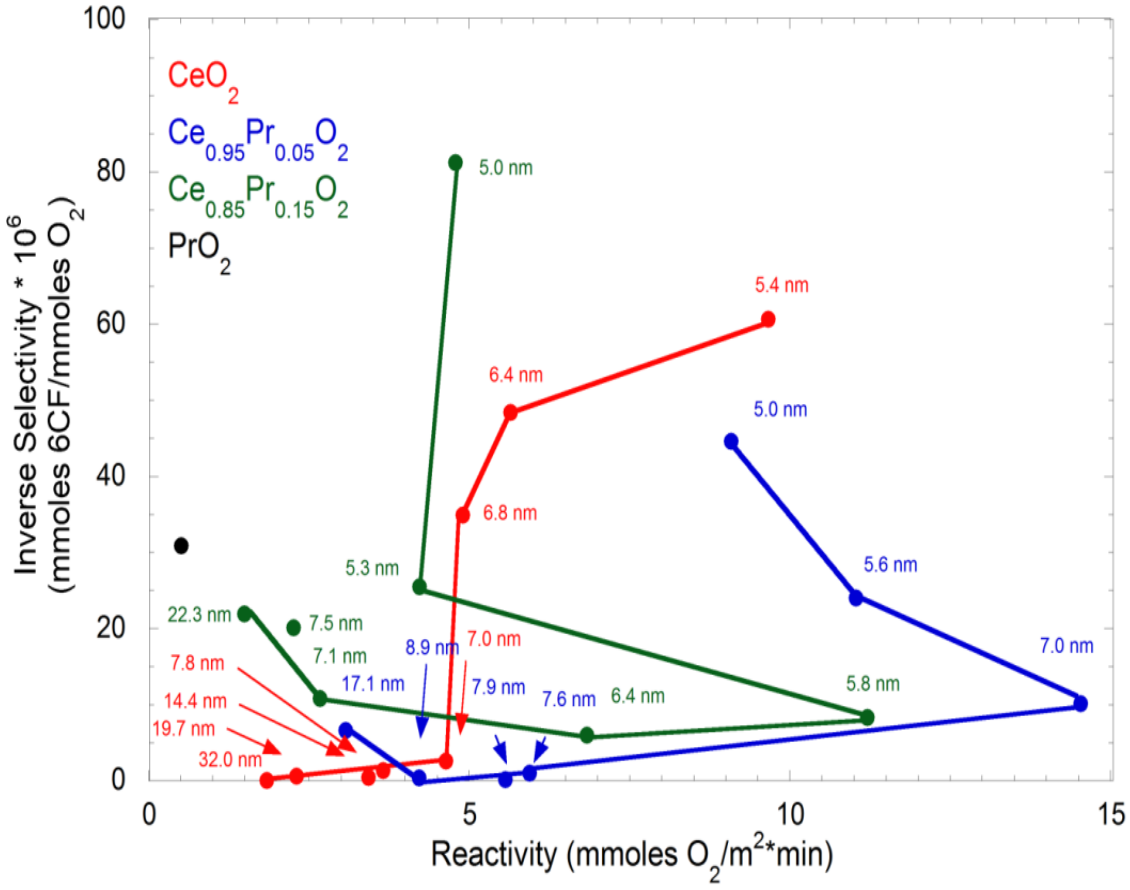

Figure 1. Inverse selectivity versus activity for peroxide decomposition by different particle sizes of cerium oxide (red), $Ce_{0.95}Pr_{0.05}O_2$ (blue), $Ce_{0.85}Pr_{0.15}O_2$ (green), and bulk PrO_2 (black). Particle sizes for the different doped and undoped cerium oxides are listed beside the data points.

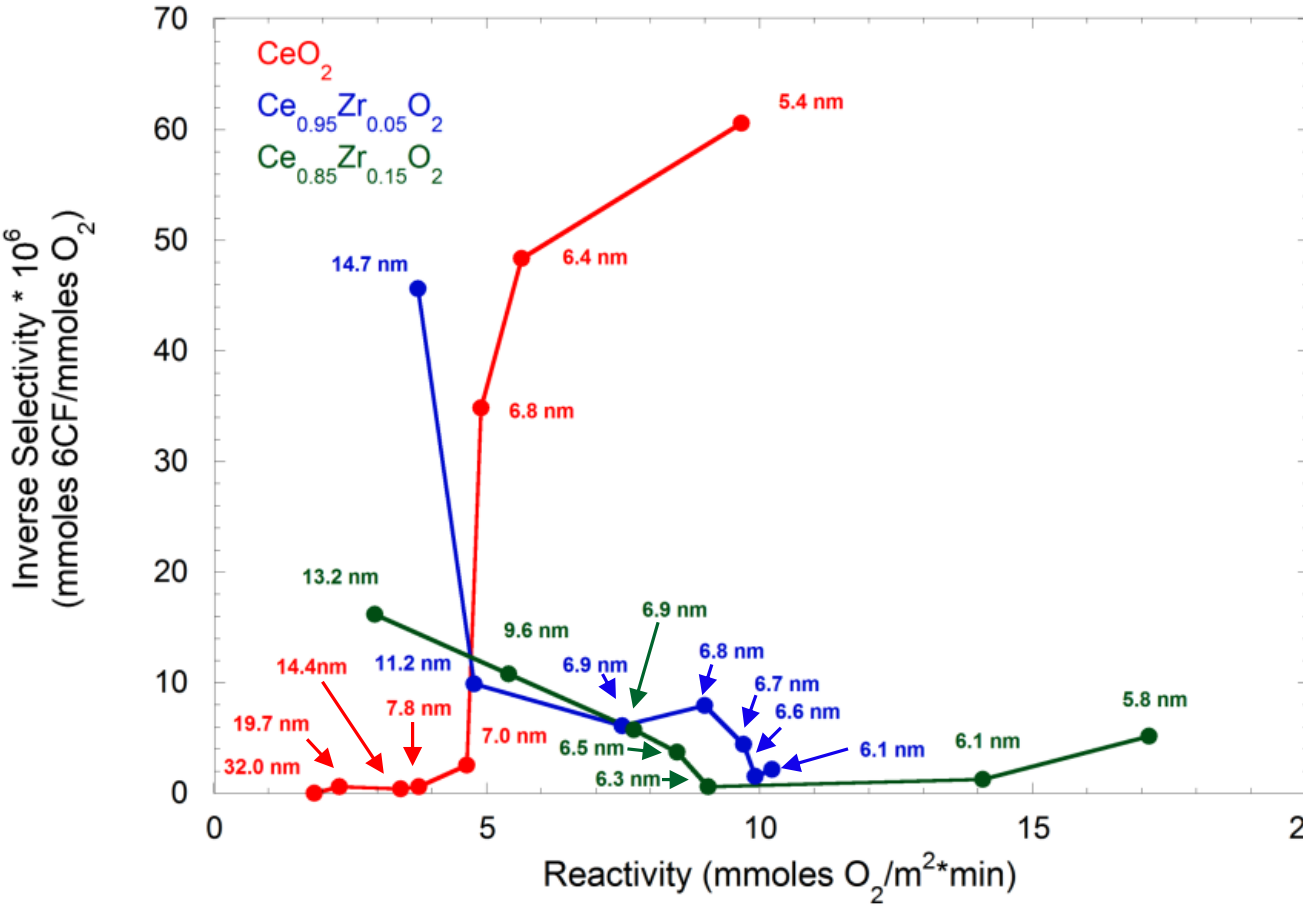

Figure 2. Inverse selectivity versus activity for peroxide decomposition by different particle sizes of cerium oxide (red), $Ce_{0.95}Zr_{0.05}O_2$ (blue), and $Ce_{0.85}Zr_{0.15}O_2$ (green). Particle sizes for the different doped and undoped cerium oxides are listed beside the data points.

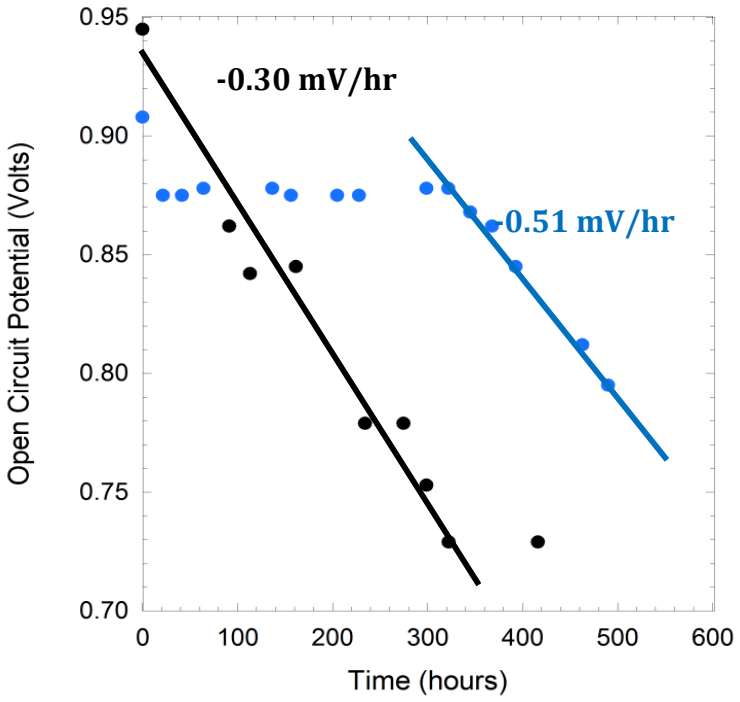
-0.30 mV/hr
-0.51 mV/hr
Open Circuit Potential (Volts)
Time (hours)
0.95
0.90
0.85
0.80
0.75
0.70
0
100
200
300
400
500
600

a

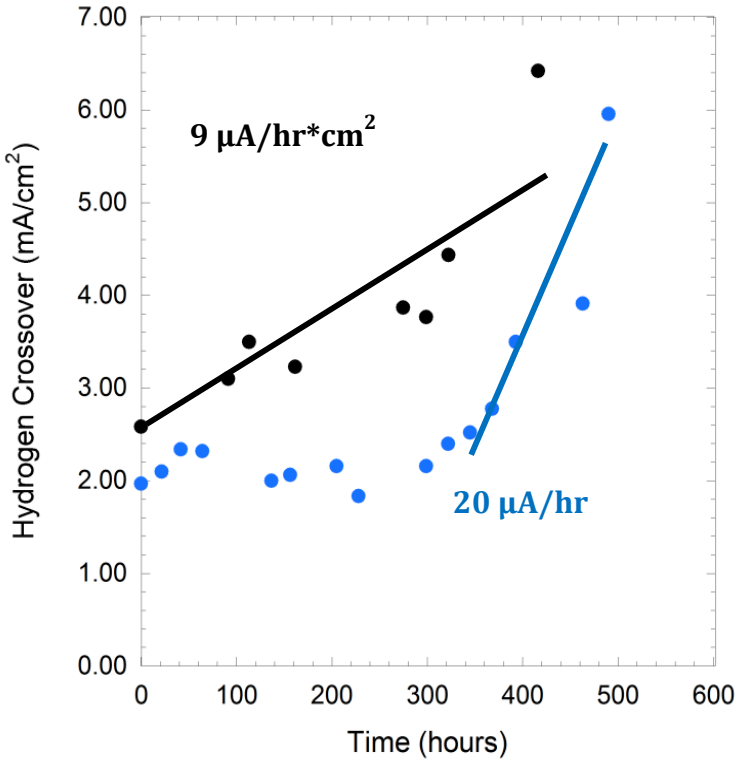
9 µA/hr*cm2
20 µA/hr
Hydrogen Crossover (mA/cm2)
Time (hours)
7.00
6.00
5.00
4.00
3.00
2.00
1.00
0.00
0
100
200
300
400
500
600

b

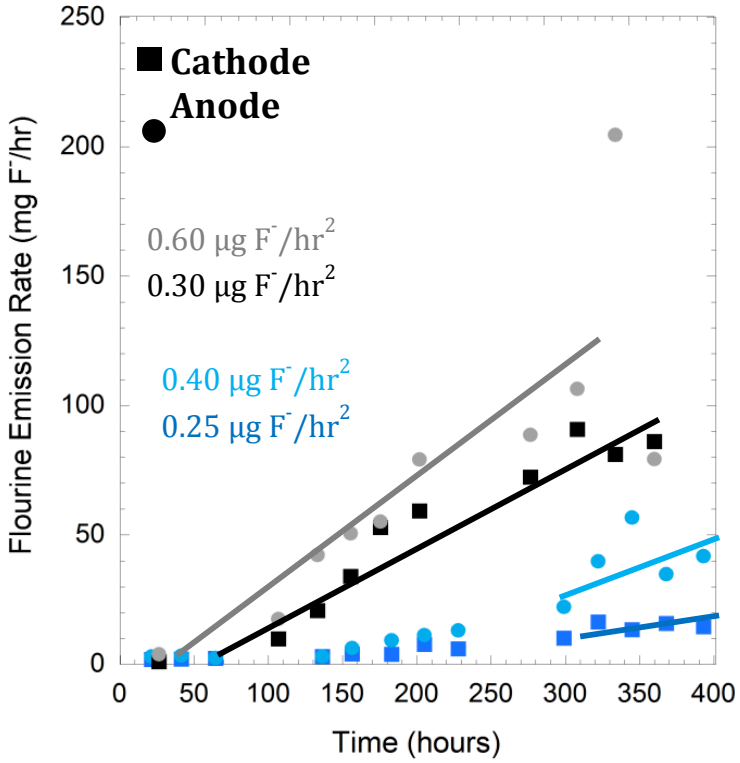

c

Figure 3. Un-stabilized membrane fuel cell open circuit voltage accelerated stress test with 7nm ceria particles (blue) addition to cathode versus XL un-stabilized membrane fuel cell (gray black) a) open circuit voltage, b) hydrogen crossover, c) fluorine ion emission.

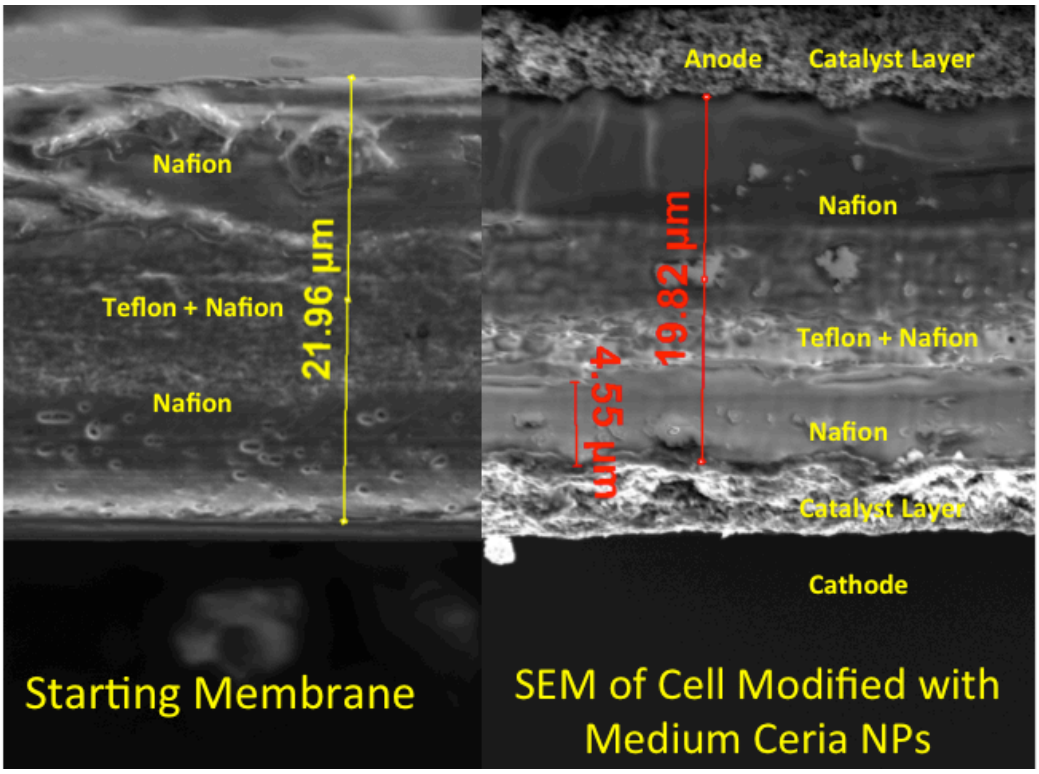

Figure 4. SEM images of fuel cell membrane electrode assembly before and after 500hrs testing.

50 cm^2 Fuel Cell Type	Rate of OCV Loss (mV/hr)	Rate of Hydrogen Crossover (µAmp/cm^2*hr)	Rate of Fluorine Emission Rate Increase (mg F^-/hr^2)	
			Anode	Cathode
XL membrane un-stabilized	0.30	9	0.30	0.60
XL membrane stabilized	0.0	0.0	.004	0.024
Large 38 nm Ceria	0.16	0.9	0.06	0.11
Medium 7 nm Ceria (<350 hrs)	0.0	0.0	0.04	0.09
Medium 7nm Ceria (>350 hrs)	0.51	20	0.25	0.40
Small 5nm Ceria	0.44	16	0.23	0.70

Table 1. Summary of the open circuit degradation of fuels cells using un-stabilized, and Ce^{3+} ion exchange stabilized membranes versus ceria nanoparticle stabilized fuel cells.

Acknowledgments

The authors wish to acknowledge the financial support of the U.S. DOE, Energy Efficiency and Renewable Energy, Fuel Cell Technologies Office and Technology Development Manager Nancy Garland.

References

(1) Endoh, E.; Terazono, S.; Widjaja, H.et al. *Electrochem. Solid-State Lett.* **2004**, Vol 7, A209.

(2) Coms, F. D. In *Proton Exchange Membrane Fuel Cells 8, Pts 1 and 2*; Fuller, T., Shinohara, K., Ramani, V., Shirvanian, P., Uchida, H., Cleghorn, S., Inaba, M., Mitsushima, S., Strasser, P., Nakagawa, H., Gasteiger, H. A., Zawodzinski, T., Lamy, C., Eds. **2008**; Vol. 16, p 235.

(3) Endoh, E. In *Proton Exchange Membrane Fuel Cells 8, Pts 1 and 2*; Fuller, T., Shinohara, K., Ramani, V., Shirvanian, P., Uchida, H., Cleghorn, S., Inaba, M., Mitsushima, S., Strasser, P., Nakagawa, H., Gasteiger, H. A., Zawodzinski, T., Lamy, C., Eds. **2008**; Vol. 16, p 1229.

(4) Prabhakaran, V: Arges,C. G.; and Ramani, V; *Proceedings of the National Academy of Sciences of the United States of America*, **109**, 1029 (**2012**).

(5) Banham, D.; Ye, S.; Cheng, T.et al. In *224th Electrochemical Society Meeting*; ECS: San Francisco, CA, **2013**.

(6) Stewart, S. M.; Borup, R.; Wilson, M.,et al. *ECS Electrochem. Lett.* **2014** Vol 3, 4, F19-F22